

Size Effects in Nanoparticle Catalysis at Nanoparticle Modified Electrodes: the Interplay of Diffusion and Chemical Reactions

Chuhong Lin, Richard G. Compton*

Department of Chemistry, Physical and Theoretical Chemistry Laboratory, Oxford University,
South Parks Road, Oxford OX1 3QZ, UK

*To whom correspondence should be addressed

Email: richard.compton@chem.ox.ac.uk

Phone: +44 (0) 1865 275957

Fax: +44 (0) 1865 275410

Abstract

Electron transfer reactions mediated via nanoparticles immobilized on an electrode surface are considered in respect of catalytic processes in which solution phase species are either oxidized or reduced to form products exclusively via electron transfer with negligible reaction at the underlying supporting electrode. Specifically simulation is used to explore the effect of the nanoparticle size both for individual nanoparticles as well as ensembles of nanoparticles and a kinetic diagram developed. For a single nanoparticle its size controls the rates of diffusion of species to and from the particle so that the relative extent of the catalysis is reduced for larger particles. For an array of nanoparticles the response of the whole is sensitive not only to the particle size but also to the particle coverage since the inter-particle distance influences the extent, or otherwise, of the local overlap of the diffusion layers of neighbouring particles and hence also the extent of the catalysis. Both particle size and coverage are essential parameters to consider in evaluating possible electrocatalytic nanoparticles.

Introduction

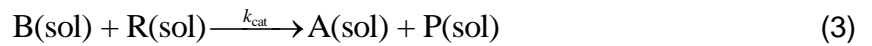
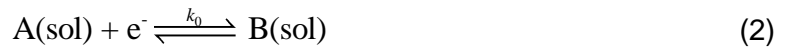
The explosion of interest in energy transformation technologies driven by societal demands as well as the need for designing sensitive and selective chemical sensors has driven major activity in the area of the controlled and informed modification of electrode surfaces so as to catalyse processes which are otherwise electrochemically slow. Examples of such processes range from the reduction of oxygen to water in aqueous solution as is vital for many fuel cells,¹⁻² to the fixing of nitrogen to form ammonia³ and the chemical sensing of analytes such as glucose and ascorbic acid.⁴ One, now frequent, approach to the surface modification is the immobilization of a layer of nanoparticles on the electrode surface. Often these function by conducting electrons to or from the electrode whilst also offering new active sites for reaction and hence promoting a catalytic reaction. In this way, at the very least, expensive materials on the supporting and inexpensive substrate electrodes (often carbon based) are used in minimal quantities but in other cases specific nano-effects are seen, most notably quantum confinement effects, altering the electronic properties of the nanoparticle material in comparison with the bulk analog but also altered relative adsorption deriving from the much changed step to terrace ratio of the particle surface. Examples of both positive and negative catalysis have been documented.⁵⁻⁷

Nanoparticle modified electrodes can be optimised by altering the coverage of the particle along with the particle size and possibly shape. In particular, the size can influence the quantum confinement and adsorption effects. At the same time it is important to appreciate that particle size and coverage can profoundly influence the rates of mass transport of reactants and products to and from the active surface.⁸⁻⁹ This is especially important in the area of multi-electron process where one or more solution phase intermediates are formed, as in the sequential reduction of oxygen via hydrogen peroxide to form water.¹⁰ Then in the simplest case of a so-called ECE process (in the Testa and Reinmuth notation E corresponds to an electron transfer and C to a chemical step):



where A, B, C and Products in Eq.(1) are all solution species, shrinking the particle size can, especially at low particle coverages encourage the loss of B into bulk solution via divergent diffusion. As this loss becomes competitive in rate with the chemical step, the reaction can ‘switch’ from a two electron to a one electron process. Thus for small particles where the radial diffusion predominates, the product of the reaction is B whereas for larger particles, with relatively more linear diffusion, the product is C. Such considerations have been used to explain the nano-toxicity of silver nanoparticles where toxic hydrogen peroxide is formed with tiny particles whereas water is formed from the reduction of oxygen at larger particles with in each case the electrons deriving from the dissolution of the silver to Ag^+ encouraged by chemical complexation with the cell.¹¹⁻¹² Similar ideas underpin the use of electrodes modified with the enzyme catalyse at high coverage for the four electron reduction of oxygen in comparison with the two electron formation of hydrogen peroxide.¹³

In the current work, we explore computationally using simulation the effects of particle size on a catalytic (so-called EC'¹⁴) reaction occurring at a nanoparticle surface. In this mechanism, the key steps are as follow:



where A and B are the redox couple, R and P are the reactant and the product of the catalytic process, k_0 is the standard electron transfer rate constant, k_{cat} is the second-order catalytic rate constant. All the reactive species are dissolved in the solution and there is no adsorption on the electrode surface.

We have selected this system partly since it is the basis of both the technique of chemical etching for electrochemical etching for electrochemical machining with nanoscale accuracy¹⁵ and of a wide diversity of electrochemical sensor, for example, sensors for detecting glucose (diabetes testing),⁴ ascorbic acid,¹⁶ gases¹⁷⁻¹⁸ and alcohols.¹⁹⁻²¹ This system is also selected with the aim of unveiling the factors which control the observed catalytic response. In this way we build on previous work which characterises the catalysis process via voltammetric techniques,²²⁻²⁵ to develop an appreciation of the factors controlling catalysis at nanoparticle modified electrodes and in particular, consider particle size, particle shape and the inter-particle separation on the electrode surface. The first two of those factors are often explored by experimentalist but the last is relatively neglected. In particular, by comparing different particle shapes, notably discs, spheres and hemispheres, we show that the homogeneous catalytic reactions on particles with different geometries have altered and size-dependent catalytic responses, especially at low surface coverages. Moreover, we consider the role of the particle separation to show that this too has a profound physical impact on the catalytic behaviour and present data to show that it needs to be considered alongside the other two parameters in understanding particle catalytic behaviour. Last we note that, without simulations of the type presented, resolution of the three different parameters is difficult especially if resorting solely to pure empirical experimentation.

2 Theory and Simulation

In this section, the theoretical model and the numerical simulation applied for the homogeneous catalytic reaction on the nanoparticle will be developed. To model the reaction on the nanoparticle, the reaction is first simulated on a single nanoparticle located on a conductive, inert supporting electrode. Then an ensemble of nanoparticles immobilized on the supporting electrode will be considered. Two particle geometries for the nanoparticle, spheres and discs, are taken into consideration.

2.1 Theoretical Model

In the electron transfer step (2) of the homogeneous catalytic reaction, assuming the electron transfer is fast, the surface concentration of the redox couple can be described by the Nernst Equation:

$$\frac{c_{A, \text{surf}}}{c_{B, \text{surf}}} = \exp\left(\frac{F\eta}{RT}\right) \quad (4)$$

where F is the Faraday constant, R is the ideal gas constant, T is absolute temperature. The overpotential η equals to the difference between the applied potential E and the formal potential E_f . Note that no reaction is assumed on the supporting electrode where the overpotential required for reaction is assumed infinite. In contrast the use of Eq.(4) presumes a negligible overpotential reflects the catalytic properties of the nanoparticle.

The reaction flux for A on the nanoparticle surface is expressed as:

$$j_A = -D_A \frac{\partial c_A}{\partial \vec{n}} \Big|_{\text{surf}} \quad (5)$$

where \vec{n} is the vector perpendicular to the electrode surface, D is the diffusion coefficient. A reflective boundary condition is applied for the concentration gradient of R on both the nanoparticle and the inert supporting electrode surface:

$$\left. \frac{\partial c_R}{\partial n} \right|_{\text{surf}} = 0 \quad (6)$$

In the theoretical model, it is assumed that the homogeneous catalytic reaction Eq.(3) occurs only in the solution and the reactant R is inert on the electrode surface. Although the zero-gradient boundary condition for R on the electrode surface at first sight appears in contradiction to the fact that R can react in the solution layer just above the electrode, the zero-gradient boundary condition for species R has to be applied, otherwise the simulation deviates from our theoretical chemical model. In addition, the grid space in the simulation model between the first solution layer and the electrode surface is small enough to reduce any inaccuracy caused by the separation of the zero-gradient boundary condition on the electrode and the homogeneous reaction in the solution. The same reflective boundary condition is also applied for the redox species on the supporting electrode.

Assuming that there is enough amount of electrolyte in the solution and the experimental time is rather short, the influence of the migration and convection can be ignored.²⁶⁻²⁷ The change of the concentrations in the solution is driven by both diffusion and the homogeneous catalytic reaction:

$$\frac{\partial c_A}{\partial t} = D_A \nabla^2 c_A + k_{\text{cat}} c_B c_R \quad (7)$$

$$\frac{\partial c_R}{\partial t} = D_R \nabla^2 c_R - k_{\text{cat}} c_B c_R \quad (8)$$

Provided that $D_A = D_B$, the concentration of B in the above equations can be replaced by $c_A^* - c_A$, where c_A^* is the bulk concentration of A. By solving the partial differential equations (7) and (8), the concentrations of A and R can be derived. Therefore, the current can be calculated by:

$$I = \int F j_A dS \quad (9)$$

where S refers to the surface area of the electrode.

In order to discover the potential dependence of the current measured at the single nanoparticle, we simulate the current response to the potential which is swept over a range of interest. Note that in cyclic voltammetry, when the sweep rate of the potential is slow, a steady-state response is established on a time scale of $\tau = r_{\text{el}}^2/D$ where r_{el} is the nanoparticle radius and $D \approx D_{\text{ox}} \approx D_{\text{red}}$. In particular for nanoparticles, the steady-state is established almost instantaneously but the treatment below allows in principle for application to particles of any size and any applied potential. To correspond to common electrochemical practice we also consider a reverse potential sweep and generate a cyclic voltammogram to characterise the homogeneous catalytic reaction on nanoparticles. To simulate this, the overpotential η is not a constant but varies as a function of the experimental time t :

$$\eta = \begin{cases} \eta_{\text{ini}} + vt & t \leq \frac{\eta_{\text{rev}} - \eta_{\text{ini}}}{v} \\ \eta_{\text{rev}} + v \left(t - \frac{\eta_{\text{rev}} - \eta_{\text{ini}}}{v} \right) & t > \frac{\eta_{\text{rev}} - \eta_{\text{ini}}}{v} \end{cases} \quad (10)$$

where $[\eta_{\text{ini}}, \eta_{\text{rev}}]$ is the sweeping window and v is the scan rate.

2.2 Numerical Simulation

In this paper, two different geometries of the nanoparticle are simulated: a sphere and a disc. As the diffusion is related with the geometry of the electrode system, both geometries are modelled and compared to explore the influence of the nanoparticle geometry on the homogeneous catalytic reaction. As the simulation for a sphere which is located on the supporting substrate is more complex and time-consuming than that for a planar disc, the possibility of simplifying the geometry of a sphere into a disc is also examined. The illustration of the geometries and the simulation spaces for the two geometries are shown in Figure 1. As the geometry is symmetric, a two-dimension cylindrical coordinate system (r, z)

is applied, where r is the radial direction parallel to the supporting substrate and z is perpendicular to r . The calculation grids are built by the same method introduced in our previous work.²⁸

The ensemble of nanoparticles modified on the supporting substrate is a nanoparticle array. Here the regular array is applied to simulate the nanoparticle modified electrode. For the regular array model, the inert substrate is split into a regular distribution of cells, where each cell contains one nanoparticle and, assuming close packing, each cell has the shape of a hexagon. As all the cells are equivalent, only one cell needs to be simulated in order to explore the electrochemical behaviour of the whole nanoparticle array. Figure 2 shows an illustration of the regular nanoparticle array and the diffusion domain approximation of one nanoparticle, where d is the average distance between two nearby nanoparticles and r_{domain} is the radius of the circle diffusion domain area. In the diffusion domain approximation, the hexagonal cell of Figure 2b has the same area with a circular cell.²⁹ Therefore, the coverage of nanoparticles are defined by $(r_{\text{el}}/r_{\text{domain}})^2$. The current measured from the array equals $n_{\text{domain}}I$. I is the current detected from one nanoparticle. n_{domain} is the number of the nanoparticles and $n_{\text{domain}} = (r_{\text{sup}}/r_{\text{domain}})^2$, where r_{sup} is the size of the substrate electrode. The simulation space for one nanoparticle in the array is the diffusion domain and similar calculation grids are built as applied in Figure 1. In contrast to the single nanoparticle, when simulating the array, as the two nearby cells are symmetric, there is no flux passing through the boundary of each simulation cell. The concentration gradient for solution species is zero at $r = r_{\text{domain}}$.

The resulting problem was solved numerically by means of the Newton-Raphson method and the alternating direction implicit (ADI) method, the details of which can be found in the literature.³⁰ The simulation programmes were written in Matlab R2016a and performed using an Intel(R) Xeon(R) 3.60G CPU. The runtime was approximately 1 hour for one cyclic voltammogram and the simulation results were converged.³¹

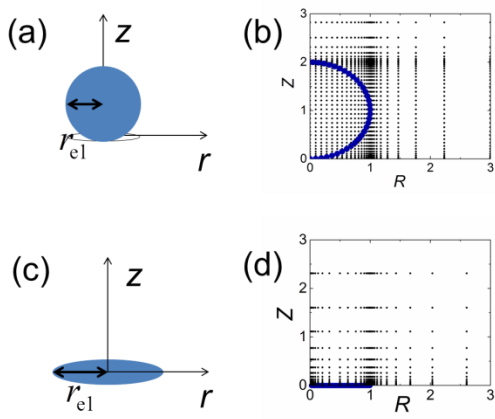


Figure 1 Illustration of the geometry and calculation grids for sphere (a, b) and disc (c, d) nanoparticles located on the supporting substrate. The blue lines in b and d show the position of the electrode surface. r_{el} is the radius of the electrode. In b and d, the normalized Z is equal to z/r_{el} and R is r/r_{el} .

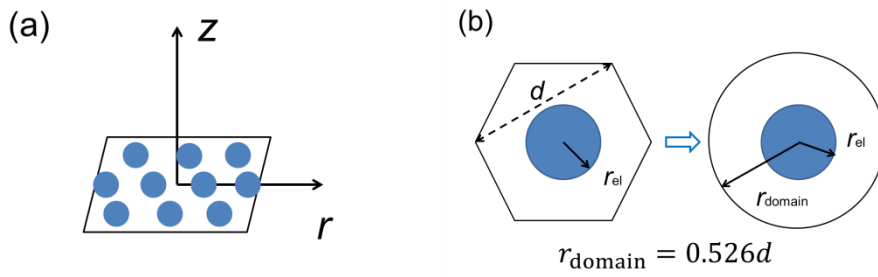


Figure 2 (a) Regular distribution of the nanoparticles on the supporting surface; (b) Diffusion domain approximation for one cell.

3 Results and Discussion

For the homogeneous catalytic reaction, as both the redox catalyst A and the reactant R are assumed to be solution phase species, the reaction rate is determined by both the diffusion from the bulk solution to the nanoparticle surface and the catalytic kinetics. In this section, the current-potential response of the homogeneous catalytic reaction on both individual nanoparticles and nanoparticle ensembles are simulated. The size effects on the electron transfer efficiency and mechanism are explored, providing information on the interplay between the diffusion and the kinetics in the homogeneous catalytic system.

3.1 Size Effects on Electron Transfer Efficiency on Individual Nanoparticles

Due to the convergent diffusion, the current-potential dependence for an electron-transfer reaction on a nanoparticle is an S-shape curve with the limiting current controlled by diffusion. The apparent (or ‘effective’) number of electrons transferred in the reaction n_e can be determined from $I_{ss} / I_{ss,1e}$, where I_{ss} is the measured steady-state current at high overpotentials and $I_{ss,1e}$ is the theoretical value of the diffusion-limited, one-electron-transfer reaction seen in the absence of any catalysis. Dependent on the nanoparticle geometry, $I_{ss,1e}$ can be expressed as:

$$I_{ss,1e} = \begin{cases} 4FD_A c_A^* r_{el} & \text{disc nanoelectrode} \\ 4\pi \ln 2 FD_A c_A^* r_{el} & \text{sphere nanoelectrode} \end{cases} \quad (11)$$

When the electron transfer process is followed by a chemical step catalysed by the redox species, the current measured on the electrode will be promoted due to the cycling of the redox catalyst. Therefore, the steady-state current as well as the effective number of electrons n_e will be affected as well. Figure 3 shows the influence of the catalytic process (Eq.(3)) on the current-potential dependences of the catalytic reaction on a spherical nanoparticle. In Figure 3a and 3b, the current-potential dependences are simulated with various catalytic rate constants k_{cat} and concentrations of the reactant in the bulk solution

c_R^* . It is observed in Figure 3a that with the increase of k_{cat} , the “half-wave potential” (defined as the potential where $I = \frac{1}{2} I_{ss}$) shifts positively and the maximum steady-state current increases. Figure 3b shows that the amount of the reactant added in the solution has a significant effect on the value of I_{ss} , which alters the effective number of electrons transferred in the homogeneous catalytic reaction. In the simulation of various k_{cat} , it is found that the steady-state current cannot infinitely increase with k_{cat} . When the catalytic process is ultrafast and the steady-state current shows independence of k_{cat} , the diffusion of A and R becomes the rate-determining factor for such a reaction and the homogeneous catalytic reaction can be approximated as a two-step electron-transfer reaction:



The steady-state current of Eq.(12) is the sum of the diffusion limited steady-state currents for the electron transfer steps A/B and R/P:

$$I_{ss} = I_{ss,A/B} + I_{ss,R/P} \quad (13)$$

Therefore, the effective n_e for the fast ($k_{cat} \gg 1$ and I_{ss} is independent of k_{cat}) homogeneous catalytic reaction becomes:

$$n_{e,max} = 1 + \frac{D_R C_R^*}{D_A C_A^*} \quad (14)$$

This value is also the maximum number of transferring electrons that can be detected for a homogeneous catalytic reaction on any size of the nanoparticle.

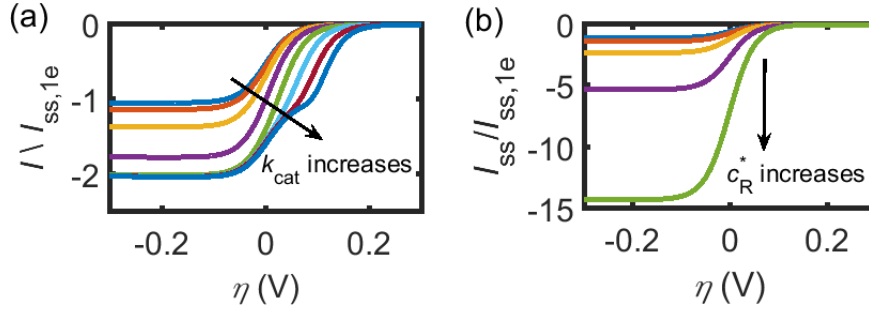


Figure 3. Current-potential dependences of homogeneous catalytic reactions on a spherical nanoparticle: (a) under various k_{cat} . From top to bottom, the value of k_{cat} for each plot increases from 0.1 to $10^6 \text{ mM}^{-1}\text{s}^{-1}$. In the simulation, $c_A^*=c_R^*=1 \text{ mM}$, $D_A = D_R = 10^{-10} \text{ m}^2 \text{ s}^{-1}$, $r_{\text{el}} = 1000 \text{ nm}$, $k_0 = 10^3 \text{ m s}^{-1}$ and $\alpha = \beta = 0.5$; (b) under various c_R^* . From top to bottom, the value of c_R^* for each plot increases from 0.1 to 10^3 mM . k_{cat} is $10 \text{ mM}^{-1}\text{s}^{-1}$ and other simulation conditions are the same as above. The sweep of the overpotential starts from 0.3 V.

On the other hand, when the mass transport of the reactant R is much faster than the redox species A, the concentration change of R can be ignored and in the solution $c_R \approx c_R^*$. At steady state, the diffusion equation of the redox catalyst A then becomes:

$$\frac{\partial c_A}{\partial t} = D_A \nabla^2 c_A + k_{\text{cat}} (c_A^* - c_A) c_R^* = 0 \quad (15)$$

To simplify the equation, we first solve the equation on an isolated sphere electrode where only the radial direction r needs to be taken into consideration. The concentration variation on the radial direction is:

$$c_A(r) = c_A^* - \frac{c_A^* r_{\text{el}}}{r} \exp\left(-\sqrt{\frac{k_{\text{cat}} c_R^*}{D_A}} (r - r_{\text{el}})\right) \quad (16)$$

According to Eqs.(5) and (9), the steady-state current then can be solved:

$$I_{ss} = -FSD_A \left. \frac{dc_A}{dr} \right|_{r=r_{el}} = -FSD_A \left(\frac{c_A^*}{r_{el}} + c_A^* \sqrt{\frac{k_{cat} c_R^*}{D_A}} \right) \quad (17)$$

where $S = 4\pi r_{el}^2$ is the surface area of the nanoparticle. Thus the effective n_e in this case are limited by the catalytic rate and the electrode size:

$$n_e = 1 + r_{el} \sqrt{\frac{k_{cat} c_R^*}{D_A}} \quad (18)$$

Note that Eq.(18) only works for isolated sphere electrodes and the geometry of the electrode will also affect the value of n_e , which will be discussed later.

For more general cases, combining our simulation work with reports in the literature,^{23, 32-33} the number of transferring electrons for the catalytic reaction is found to be dependent on two combined parameters: γ_{AR} and K_{cat}

$$\gamma_{AR} = \frac{c_R^* D_R}{c_A^* D_A} \quad (19)$$

$$K_{cat} = \frac{k_{cat} c_R^* r_{el}^2}{D_A} \quad (20)$$

where γ_{AR} is related to the excess of the reactant relative to the redox catalyst and K_{cat} reflects the size effects on the catalytic reaction rate. The variation of the nanoparticle size is reflected in the parameter K_{cat} .

Taken the geometry influence into consideration, the number of electrons transferred, n_e , can be approximated as a function of γ_{AR} and K_{cat} :

$$n_e = \frac{I_{ss}}{I_{ss,1e}} \approx 1 + \frac{\sqrt{K_{cat}}}{\delta_{geo} + \frac{\sqrt{K_{cat}}}{\gamma_{AR}}} \quad (21)$$

where δ_{geo} is a geometry factor dependent on the nanoparticle shape and location. δ_{geo} is $4/\pi$ for a planar nanoparticle on an inert supporting electrode and $\ln 2$ for the corresponding spherical case. From this approximate expression, it is apparent that both the size and the geometry of the nanoparticle can affect the apparent number of electrons transferred of the homogeneous catalytic reaction.

We calculate the kinetic diagrams of n_e from both disc and sphere nanoparticles as the function of K_{cat} and γ_{AR} from both the simulation programme and the approximation equation (Eq.(21)). Figure 4 shows the diagrams from the sphere nanoparticle of simulated $n_{e,\text{sim}}$ (Figure 4a), $n_{e,\text{app}}$ calculated from Eq.(21) (Figure 4b), and the difference between the

simulation and the approximation results $\frac{|n_{e,\text{sim}} - n_{e,\text{app}}|}{n_{e,\text{sim}}}$ (Figure 4c). The approximation fits

the simulation results well when K_{cat} and γ_{AR} are not large. In the kinetic diagrams Figure 4a and 4b, a dashed line divides the diagram into two, corresponding to different dominant processes for the catalytic reaction on a nanoparticle. In the K_{cat} regime, as the catalytic process is relative fast, the number of electrons transferred in the reaction is limited by the mass transport of the reactant R; whereas in the γ_{AR} regime, the supply of the reactant is sufficient and the limiting factor becomes the catalytic reaction rate. When the nanoparticle is so tiny that $K_{\text{cat}} \ll 1$, even under rather large value of γ_{AR} , only one electron corresponding to the redox step (the E step) is seen. As the catalytic rate depends on the square of the nanoparticle size, r_{el}^2 , the variation of the nanoparticle size can dramatically affect K_{cat} and hence the reaction as a whole. It can be observed from the diagrams that compared to the mass transport, the catalytic kinetics is very sensitive the variation of the nanoparticle size.

Figure 5 shows the simulation and approximation results for the catalytic reaction on the disc-shape nanoparticle. The kinetic diagram of $n_e(\gamma_{\text{AR}}, K_{\text{cat}})$ simulated from a nanodisc also can be divided into two regimes: K_{cat} and γ_{AR} , where the catalytic rate and the diffusion dominate. However, even though the kinetic diagrams show similar trends in Figures 4 and 5, the difference in geometry affects the value of the steady-state current and the measured

n_e for the homogeneous catalytic reaction on the individual nanoparticle, as indicated in Eq.(21). Therefore, for the homogeneous catalytic reaction on individual nanoparticle, the geometry factor cannot be ignored and the electron-transfer efficiency is affected by the shape of the nanoparticle.

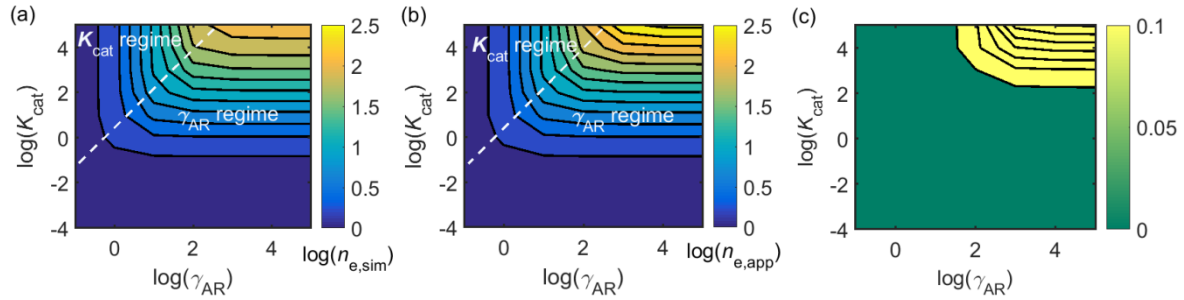


Figure 4 n_e of homogeneous catalytic reactions on a nanosphere: (a) Simulation $n_{e,sim}$ under various K_{cat} and γ_{AR} . (b) Approximation $n_{e,app}$ under various K_{cat} and γ_{AR} . (c)

Difference between the simulation and approximation results $\frac{|n_{e,sim} - n_{e,app}|}{n_{e,sim}}$.

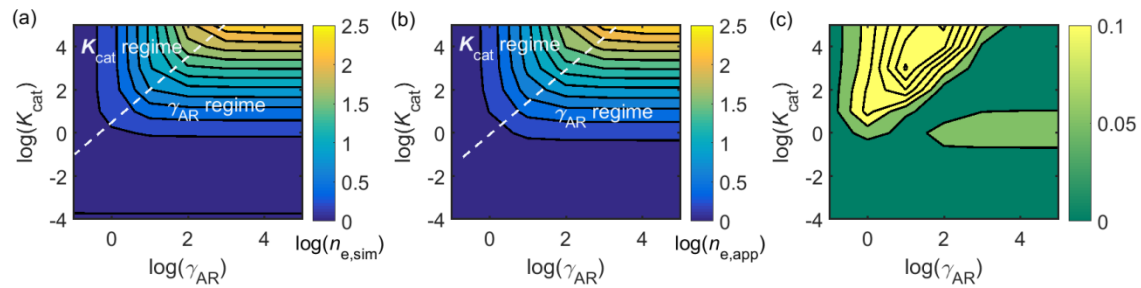


Figure 5 n_e of homogeneous catalytic reactions on a nanodisc: (a) Simulation $n_{e,sim}$ under various K_{cat} and γ_{AR} . (b) Approximation $n_{e,app}$ under various K_{cat} and γ_{AR} . (c) Difference

between the simulation and approximation results $\frac{|n_{e,sim} - n_{e,app}|}{n_{e,sim}}$.

3.2 Size Effects on the Detection of Electron Transfer Mechanism

As discussed above, the catalytic reaction with an ultrafast catalytic process (large K_{cat}) can be regarded as two one-electron-transfer reactions and the effective number of transferring electrons varies as a function of γ_{AR} . Figure 6 shows the current-potential dependence of the catalytic reaction on the nanosphere with large values of K_{cat} under various γ_{AR} . The values of K_{cat} used in the examples are 10^3 (blue lines), 10^4 (red lines) and 10^5 (yellow lines) and γ_{AR} are 5.0 (Figure 6a), 1.0 (6b) and 0.1 (6c), respectively. As shown in Figure 6, when the value of K_{cat} is large enough that the steady-state current is determined by the diffusion of the redox catalyst and the reactant, the value of the normalized steady-state current equals $1 + \gamma_{\text{AR}}$, as predicted in Eq.(14).

Moreover, similar to a double electron transfer reaction (so-called ‘EE’ reaction),³⁴ a split in the current-potential curve can be observed for large values of K_{cat} in Figure 6, indicating the two separate electron-transfer processes, with that at lower overpotentials reflects the full amount of reactant R in solution with the second wave reflects the concentration of A. The separation of the two electron-transfer steps on the voltammogram is related to the value of K_{cat} : for larger K_{cat} , there is more difference between the positions of the two split waves. It is also found that the current where the separation appears depends on the value of γ_{AR} : when γ_{AR} is 5.0 (Figure 6a), the split of wave appears at $I / I_{\text{ss},1e} = 5.0$ and when $\gamma_{\text{AR}} = 1.0$ (Figure 6b), the split is at $I / I_{\text{ss},1e} = 1.0$. Figure 7 shows the voltammograms for the reaction on the nanodisc, with the same simulation conditions as applied in Figure 6. Similarly, the split of wave in Figure 7 is more noticeable when K_{cat} increases and the split position is determined by the value of γ_{AR} .

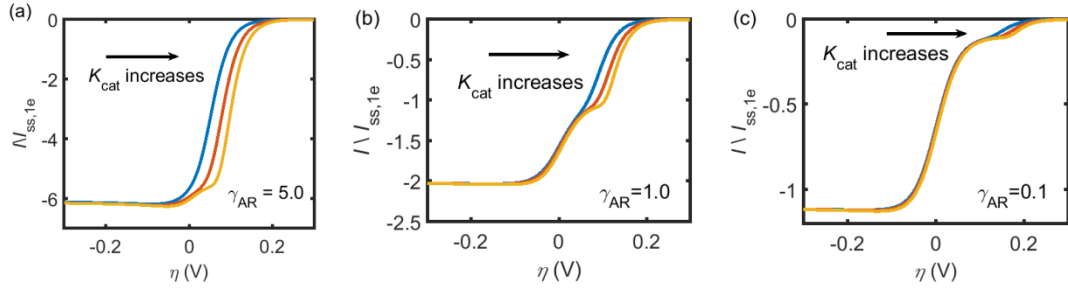


Figure 6. Voltammograms of the catalytic reaction on the nanosphere under various γ_{AR} . (a) $\gamma_{AR} = 5.0$; (b) $\gamma_{AR} = 1.0$; (c) $\gamma_{AR} = 0.1$. For each γ_{AR} , the simulation is implemented with K_{cat} equal to 10^3 (blue lines), 10^4 (red lines) and 10^5 (yellow lines). The voltage sweep starts from 0.3 V.

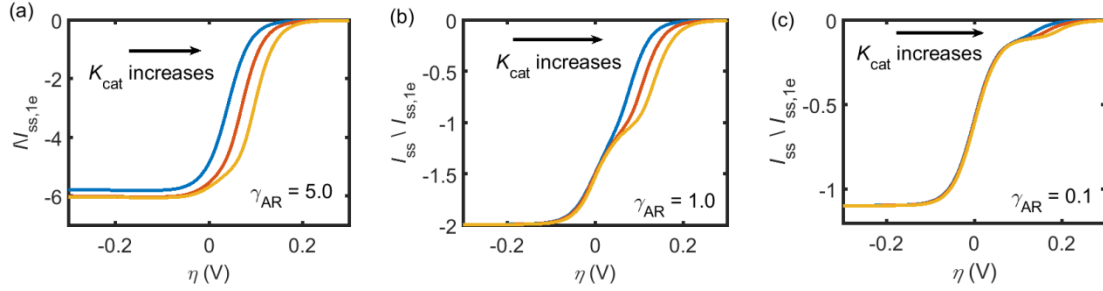


Figure 7. Voltammograms of the catalytic reaction on the nanodisc under various γ_{AR} . (a) $\gamma_{AR} = 5.0$; (b) $\gamma_{AR} = 1.0$; (c) $\gamma_{AR} = 0.1$. For each γ_{AR} , the simulation is implemented with K_{cat} equal to 10^3 (blue lines), 10^4 (red lines) and 10^5 (yellow lines). The voltage sweep starts from 0.3 V.

When the catalytic reaction is treated as a two-step electron-transfer reaction under the condition of ultrafast catalytic rate (where $n_e = 1 + \gamma_{AR}$), the split of wave provides information about the nature of the two electron-transfer steps and the number of electrons transferred in each step. From Figures 6 and 7, it is found that on both nanosphere and nanodisc, the potential dependence of the first electron-transfer process varies with K_{cat} whereas the potential dependence for the second step is always constant, indicating that the first step is the consequence of the catalytic process (Eq.(3)) while the second one corresponds to the

reversible redox reaction of A/B (Eq.(2)). It is also observed that the effective number of electrons transferred in the first step $n_{e,1st}$ is γ_{AR} and that in the second step $n_{e,2nd}$ is 1. Given that the total number of electrons transferred in the fast catalytic reaction equals $1 + \gamma_{AR}$, the same conclusion is obtained that the first electron-transfer is caused by the fast catalytic process and the second step reflects the redox step. In this case, the variation of the nanoparticle size, involved in K_{cat} , changes the overall thermodynamics of the electron transfer induced by the catalytic process and thus affects the number of electrons transferred in each step of the homogeneous catalytic reaction.

3.3 Electron Transfer Efficiency on Nanoparticle Modified Electrodes

The above text considered the catalytic response from an isolated single nanoparticle. In experimental reality, electrode surfaces are modified with ensembles of nanoparticles. In this section we consider how the presence of many nanoparticles can alter the response seen from the single particle as a result of mutually overlapping diffusion fields. Dependent on the diffusion domain size r_{domain} and the diffusion layer thickness, there are four diffusion modes on a nanoparticle modified electrode, as illustrated in Figure 8. Categories 1-4 in Figure 8 correspond to 1) the linear diffusion to a large particle surface and the diffusion condition of each particle is independent; 2) the convergent diffusion to the particle surface and the diffusion layer of each particle is independent; 3) the convergent diffusion layers of neighbouring particles overlap partly with adjacent particles; 4) the diffusion layers strongly overlap and the diffusion to the entire electrode is linear.

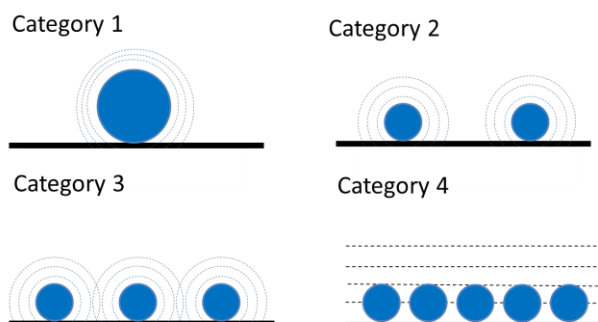


Figure 8 Four diffusion modes on the nanoparticle modified electrodes.

In the above sections, the case of independent diffusion layers (category 2) is discussed. For a nanoparticle modified electrode, when the coverage of nanoparticles is high (categories 3 and 4), the cyclic voltammogram (the current-potential response as a triangular voltage scan is applied to the electrode, see Eq.(10)) will differ from those measured from category 2, due to the overlap of the diffusion layers. However, note that in contrast to the case of single nanoparticles, significant hysteresis develops (which is only seen for extreme scan rates for a single nanoparticle). The cyclic voltammograms on the nanoparticle ensembles then become more complicated and difficult to analyse, as more variables (i.e. scan rate and nanoparticle coverage) are introduced in the system. But the key point is still to understand the interplay between the diffusion and the kinetics, which is achieved by the variation of the nanoparticle size and the catalytic rate constant in the examples of Figure 9.

Figure 9 shows the cyclic voltammograms of the catalytic reactions with various nanoparticle sizes, catalytic rates and geometries. In order to focus on the size effects of the nanoparticle on the nanoparticle array with different diffusion categories, the coverage of the nanoparticle is fixed while the nanoparticle size is altered. In Figure 9, a, b and c are simulated with the disc model and the size of nanoparticles in each panel are 10, 100 and 1000 nm, respectively. Therefore, the diffusion mode varies from category 4 of Figure 8 (fully overlapped diffusion layers) to category 3 (partly overlapped diffusion layers). In addition, to

explore how the interplay between the diffusion and the homogeneous catalysis can influence the electrochemical responses collected from the nanoparticle array, two catalytic rate constants are used in the simulation: 10^2 (blue lines) and 10^4 (red lines) $\text{mM}^{-1} \text{s}^{-1}$. Figures 9 d-f are similar to a-c but simulated with the sphere model. To examine the electron transfer efficiency for the homogeneous catalytic reaction on the nanoparticles modified electrodes, the current-potential responses are compared with those simulated from the one-electron-transfer redox reaction, which are shown by the dashed black lines in Figure 9. The current for the catalytic reaction on the nanoparticle ensemble is normalized by the forward peak current of the redox reaction $I_{\text{peak,1e}}$ in each panel.

Without the catalytic process, the diffusion mode alters when the nanoparticle size increases, as indicated by the waveshape of the redox-only cyclic voltammograms in Figure 9. As the coverage is constant, the increase of the nanoparticle size leads to larger distance between two adjacent particles and thus changes the diffusion mode from category 4 to category 3 in this case. On the other hand, the increase of the catalytic rate leads to an enhancement of the current and a shift to low overpotential in the forward sweeping, improving the electron transfer efficiency as it does on individual nanoparticles. When the catalytic process is fast, the split of waves can be observed with small nanoparticles, while the first and second split peaks correspond to the catalytic process and the mass transport limitation, respectively. The split of wave is less apparent with the increase of the nanoparticle size, as a consequence of the variation of the diffusion mode. A similar result was reported for the “EC’ reaction” on hemisphere nanoparticle arrays.²³

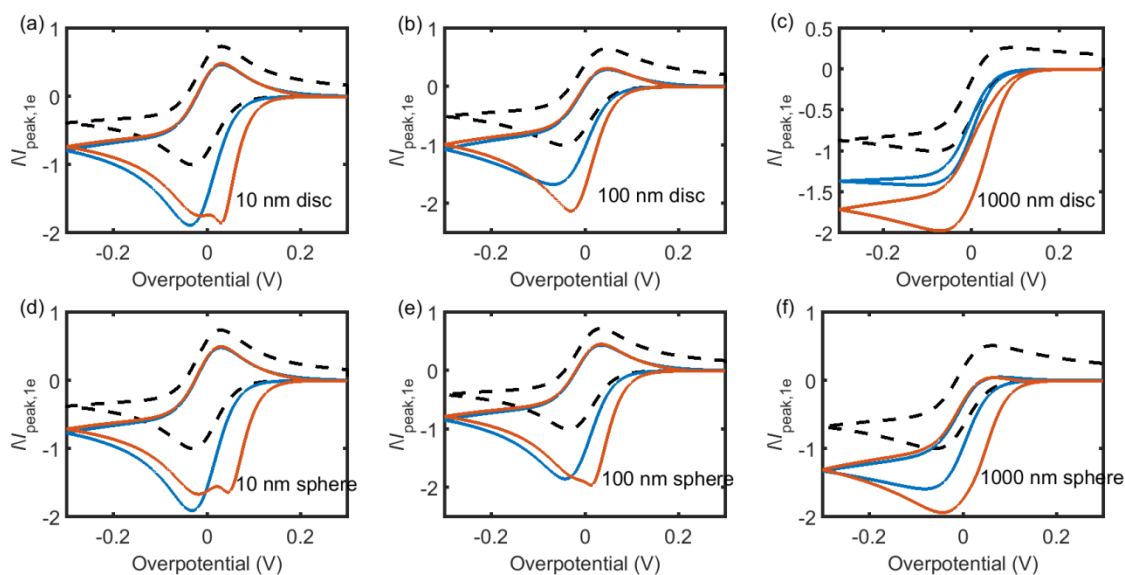


Figure 9 Current-potential responses of the catalytic reactions on nanoparticle modified electrodes. a, b and c are simulated on disc nanoparticles while d, e and f are on sphere nanoparticles. The radii of the nanoparticles are 10(a, d), 100(b, e), 1000(c, f) nm. The catalytic rate constants applied are 10^2 (shown by blue lines) and 10^4 (red lines) $\text{mM}^{-1}\text{s}^{-1}$. In the simulation, $c_R^* = c_A^* = 1 \text{ mM}$, $D_R = D_A = 10^{-10} \text{ m}^2\text{s}^{-1}$, $v = 1 \text{ V s}^{-1}$, $r_{\text{sup}} = 1 \text{ mm}$. The coverages of the nanoparticles is 4% on the supporting electrode. The dashed black lines are the current-potential responses only from the redox reaction A/B. The voltage scan starts at 0.3 V.

Figures 9a-c and 9d-f are the simulation results from the disc and sphere models. In the diffusion mode of category 4, due to the overlapped diffusion layer, there is no significant difference on the cyclic voltammograms of disc and sphere geometries, as shown in Figure 9a and 9d. However, under the same coverage, when the size of the nanoparticle increases, the geometry influence becomes more significant, indicated by the difference on the waveshape between Figures 9 b, c and e, f. For the limiting case of individual nanoparticles, the geometry can affect the measured number of electrons transferred in the homogeneous catalytic reaction. Therefore, unless the coverage of the nanoparticle is high in the ensemble, the influence of the geometry cannot be ignored. Moreover, unlike the case of a

single isolated particle, for an ensemble, a sustained, steady current cannot be realised as a consequence of the overlapping diffusion fields destroying the local convergent diffusion and hence it is essential to track spatial and temporal concentration profiles of all species if the catalytic process is to be understood. At low coverages and short time scales, different shaped particles will respond according to their surface area. But at long time scales, the diffusion layers either overlap or at least become convergent, and the electrochemical responses are not influenced much by the morphology of the nanoparticle.

The effects of changing the particle size cannot be separated from those of the particle coverage (or inter-particle separation) in an ensemble immobilized on an electrode surface. This is because the net catalytic reaction flux reflects both the chemistry and the mass transport; the latter is profoundly sensitive to the absolute inter-particle distance since this controls the overlapping or not of adjacent diffusion layers. Accordingly, experimentalists are advised to consider coverage effects as well as particle size effects when assessing the catalytic properties of new nanomaterials.

Conclusions

In this work, the influence of the nanoparticle size on the homogeneous redox catalytic reaction (EC' reaction) occurring on a nanoparticle modified electrode is explored via simulation and shown to be profound by virtue of its influence on mass transport. For the homogeneous catalytic reaction on an isolated individual nanoparticle, the steady-state current I_{ss} and the apparent number of electrons transferred in the reaction n_e are determined by γ_{AR} , the excess of the reactant to the redox catalyst, and K_{cat} , the size effects on the catalytic reaction rate. From the kinetic diagram $n_e(\gamma_{AR}, K_{cat})$, the catalytic process is found to be more sensitive to the size influence than the diffusion. On the nanoparticle arrays, under the same coverage, the increase of nanoparticle size leads to the change of the diffusion mode and the catalytic process improves the electron transfer efficiency; the response is size dependent due to the overlapping diffusion layers. For both single nanoparticles and nanoparticle arrays, the influence of geometry on the homogeneous catalytic reaction is that the disc and sphere nanoparticles have different and size-dependent current-potential responses, especially at low surface coverages.

Acknowledgement

The research is sponsored by funding from the European Research Council under the European Union Seventh Framework Programme (FP/2007-2013) / ERC Grant Agreement n. [320403].

References

1. Nie, Y.; Li, L.; Wei, Z. Recent Advancements in Pt and Pt-Free Catalysts for Oxygen Reduction Reaction. *Chem. Soc. Rev.* **2015**, *44*, 2168-2201.
2. Shao, M.; Chang, Q.; Dodelet, J. P.; Chenitz, R. Recent Advances in Electrocatalysts for Oxygen Reduction Reaction. *Chem. Rev. (Washington, DC, U. S.)* **2016**, *116*, 3594-3657.
3. Rosca, V.; Duca, M.; de Groot, M. T.; Koper, M. T. M. Nitrogen Cycle Electrocatalysis. *Chem. Rev. (Washington, DC, U. S.)* **2009**, *109*, 2209-2244.
4. Toghiani, K. E.; Compton, R. G. Electrochemical Non-Enzymatic Glucose Sensors: A Perspective and an Evaluation. *Int. J. Electrochem. Sci.* **2010**, *5*, 1246-1301.
5. Wang, Y.; Laborda, E.; Tschulik, K.; Damm, C.; Molina, A.; Compton, R. G. Strong Negative Nanocatalysis: Oxygen Reduction and Hydrogen Evolution at Very Small (2 Nm) Gold Nanoparticles. *Nanoscale* **2014**, *6*, 11024-11030.
6. Hayden, B. E. Particle Size and Support Effects in Electrocatalysis. *Acc. Chem. Res.* **2013**, *46*, 1858-1866.
7. Tang, Y.; Cheng, W. Key Parameters Governing Metallic Nanoparticle Electrocatalysis. *Nanoscale* **2015**, *7*, 16151-16164.
8. Costentin, C.; Savéant, J.-M. Catalysis at the Nanoscale May Change Selectivity. *Proceedings of the National Academy of Sciences* **2016**, 10.1073/pnas.1613406113.
9. Henstridge, M. C.; Compton, R. G. Mass Transport to Micro- and Nanoelectrodes and Their Arrays: A Review. *The Chemical Record* **2012**, *12*, 63-71.
10. Wang, Y.; Laborda, E.; Ward, K. R.; Tschulik, K.; Compton, R. G. A Kinetic Study of Oxygen Reduction Reaction and Characterization on Electrodeposited Gold Nanoparticles of Diameter between 17 nm and 40 nm in 0.5 M Sulfuric Acid. *Nanoscale* **2013**, *5*, 9699-9708.
11. Batchelor-McAuley, C.; Tschulik, K.; Neumann, C. C. M.; Laborda, E.; Compton, R. G. Why Are Silver Nanoparticles More Toxic Than Bulk Silver? Towards Understanding the Dissolution and Toxicity of Silver Nanoparticles. *Int. J. Electrochem. Sci.* **2014**, *9*, 1132-1138.
12. Plowman, B. J.; Tschulik, K.; Walport, E.; Young, N. P.; Compton, R. G. The Fate of Nano-Silver in Aqueous Media. *Nanoscale* **2015**, *7*, 12361-12364.
13. Sepunaru, L.; Laborda, E.; Compton, R. G. Catalase-Modified Carbon Electrodes: Persuading Oxygen to Accept Four Electrons Rather Than Two. *Chemistry - A European Journal* **2016**, *22*, 5904-5908.
14. Savéant, J. M. *Elements of Molecular and Biomolecular Electrochemistry: An Electrochemical Approach to Electron Transfer Chemistry*. Wiley: 2006.
15. Zhan, D.; Han, L.; Zhang, J.; Shi, K.; Zhou, J.-Z.; Tian, Z.-W.; Tian, Z.-Q. Confined Chemical Etching for Electrochemical Machining with Nanoscale Accuracy. *Acc. Chem. Res.* **2016**, *49*, 2596-2604.
16. Lertanantawong, B.; O'Mullane, A. P.; Zhang, J.; Surareungchai, W.; Somasundrum, M.; Bond, A. M. Investigation of Mediated Oxidation of Ascorbic Acid by Ferrocenemethanol Using Large-Amplitude Fourier Transformed ac Voltammetry under Quasi-Reversible Electron-Transfer Conditions at an Indium Tin Oxide Electrode. *Anal. Chem.* **2008**, *80*, 6515-6525.
17. Jeroschewski, P.; Haase, K.; Trommer, A.; Gründler, P. Galvanic Sensor for the Determination of Hydrogen Sulphide/Sulphide in Aqueous Media. *Fresenius. J. Anal. Chem.* **1993**, *346*, 930-933.
18. Jeroschewski, P.; Haase, K.; Trommer, A.; Gründler, P. Galvanic Sensor for Determination of Hydrogen Sulfide. *Electroanalysis* **1994**, *6*, 769-772.
19. Badalyan, A.; Stahl, S. S. Cooperative Electrocatalytic Alcohol Oxidation with Electron-Proton-Transfer Mediators. *Nature* **2016**, *535*, 406-410.
20. Ahn, S. D.; Fisher, A. C.; Buchard, A.; Bull, S. D.; Bond, A. M.; Marken, F. Hydrodynamic Rocking Disc Electrode Study of the Tempo-Mediated Catalytic Oxidation of Primary Alcohols. *Electroanalysis* **2016**, *28*, 2093-2103.

21. Ozawa, H.; Hino, T.; Ohtsu, H.; Wada, T.; Tanaka, K. A New Type of Electrochemical Oxidation of Alcohols Mediated with a Ruthenium–Dioxolene–Amine Complex in Neutral Water. *Inorg. Chim. Acta* **2011**, *366*, 298-302.
22. Compton, R. G.; Fisher, A. C.; Spackman, R. A. Homogeneous Catalysis of Electrochemical Reactions. Channel Electrode Voltammetry and the EC' Mechanism. *Electroanalysis* **1992**, *4*, 167-182.
23. Ward, K. R.; Lawrence, N. S.; Hartshorne, R. S.; Compton, R. G. Cyclic Voltammetry of the EC' Mechanism at Hemispherical Particles and Their Arrays: The Split Wave. *J. Phys. Chem. C* **2011**, *115*, 11204-11215.
24. Molina, A.; González, J.; Laborda, E.; Compton, R. G. Analytical Solutions for Fast and Straightforward Study of the Effect of the Electrode Geometry in Transient and Steady State Voltammeteries: Single- and Multi-Electron Transfers, Coupled Chemical Reactions and Electrode Kinetics. *J. Electroanal. Chem.* **2015**, *756*, 1-21.
25. Lin, Q.; Li, Q.; Batchelor-McAuley, C.; Compton, R. G. Use of 'Split Waves' for the Measurement of Electrocatalytic Kinetics: Methyl Viologen Mediated Oxygen Reduction on a Boron-Doped Diamond Electrode. *Phys. Chem. Chem. Phys.* **2013**, *15*, 7760-7767.
26. Ngamchuea, K.; Eloul, S.; Tschulik, K.; Compton, R. G. Advancing from Rules of Thumb: Quantifying the Effects of Small Density Changes in Mass Transport to Electrodes. Understanding Natural Convection. *Anal. Chem.* **2015**, *87*, 7226-7234.
27. Dickinson, E. J. F.; Limon-Petersen, J. G.; Rees, N. V.; Compton, R. G. How Much Supporting Electrolyte Is Required to Make a Cyclic Voltammetry Experiment Quantitatively "Diffusional"? A Theoretical and Experimental Investigation. *J. Phys. Chem. C* **2009**, *113*, 11157-11171.
28. Jiao, X.; Lin, C.; Young, N. P.; Batchelor-McAuley, C.; Compton, R. G. Hydrogen Oxidation Reaction on Platinum Nanoparticles: Understanding the Kinetics of Electrocatalytic Reactions Via "Nano-Impacts". *J. Phys. Chem. C* **2016**, *120*, 13148-13158.
29. Reller, H.; Kirowa-Eisner, F.; Gileadi, E. Ensembles of Microelectrodes. *J. Electroanal. Chem. Interfacial Electrochem.* **1982**, *138*, 65-77.
30. Compton, R. G.; Laborda, E.; Ward, K. R. *Understanding Voltammetry: Simulation of Electrode Processes*. Imperial College Press: 2013.
31. Kätelhön, E.; Compton, R. G. Testing and Validating Electroanalytical Simulations. *Analyst* **2015**, *140*, 2592-2598.
32. Savéant, J.-M.; Vianello, E. Potential-Sweep Chronoamperometry: Kinetic Currents for First-Order Chemical Reaction Parallel to Electron-Transfer Process (Catalytic Currents). *Electrochim. Acta* **1965**, *10*, 905-920.
33. Andrieux, C. P.; Dumas-Bouchiat, J. M.; Savéant, J.-M. Homogeneous Redox Catalysis of Electrochemical Reactions. *J. Electroanal. Chem. Interfacial Electrochem.* **1978**, *87*, 39-53.
34. Molina, Á.; Laborda, E.; Gómez-Gil, J. M.; Compton, R. G. Staircase, Cyclic and Differential Voltammeteries of the Nine-Member Square Scheme at Microelectrodes of Any Geometry with Arbitrary Chemical Stabilization of the Three Redox States. *J. Solid State Electrochem.* **2016**, 10.1007/s10008-016-3308-2, 1-15.

TOC Graphic

